ACS OMEGA

Open Access

http://pubs.acs.org/journal/acsodf

Article

Anti-inflammatory Lindenane Sesquiterpene Dimers from the Roots of *Chloranthus fortunei*

Xiu-Wen Yin,[‖] Jun-Jie Hu,[‖] Fu-Cai Ren, Xiang-Dong Pu, Meng-Yu Yang, Bing-Yuan Yang,* Peng Wang, and Chuan-Pu Shen*

Cite This: *ACS Omega* 2024, 9, 34869−34879

Read Online

ACCESS | Metrics & More | Article Recommendations | Supporting Information

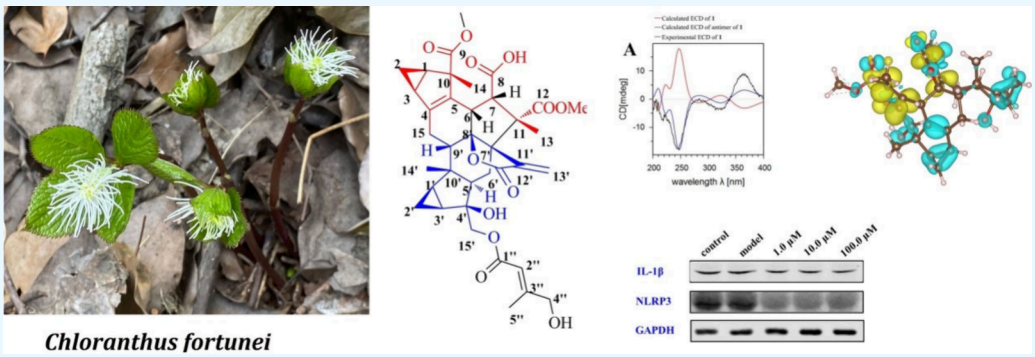

ABSTRACT: In this study, eight lindenane-type sesquiterpene dimers, including five previously undescribed sesquiterpene dimers (**1**−**5**), were isolated from the roots of *Chloranthus fortunei*, and their structures were elucidated using 1D/2D NMR, HRESIMS, and ECD calculations. Compound **1** presents the second example of a type of novel 8,9-*seco* lindenane-type sesquiterpene dimer, considered a product of 8/9-diketone oxidation. Compounds **2** and **3** represent the third and fourth examples, respectively, of this kind of C-11 methine dimer. Furthermore, compound **4** was considered as an artifact generated from the radical reaction of a known compound chlojaponilide F (**6**), which was explained by the density functional theory quantum calculation. All isolates were evaluated for their protective activity against the LPS-induced pulmonary epithelial cell line with compound **7** exhibiting the most potent bioactivity. Further *in vitro* biological evaluation demonstrated that **7** reduced the production of reactive oxygen species and interleukin-1*β*, further regulated by the expression of the NLRP3. These results show that compound **7** exhibits therapeutic potential for lung inflammatory diseases.

1. INTRODUCTION

Chloranthus is a small genus of the family Chloranthaceae, comprising 17 species, 13 of which are found in China. *Chloranthus fortunei* (A. Gray) Solms-Laub, a small herb, is distributed in various provinces in southern China. In China, the whole plants of *C. fortunei* are used as a traditional herbal medicine for treating inflammation and traumatic injuries, named as *Sidajingang*, a name derived from its characteristic four leaves.[1] This plant possesses antioxidant, anti-inflammatory, antitumor, antimalarial activities, aligning with its traditional uses.[2−4]

Inflammatory diseases pose a prevalent and serious threat to human health. If the inflammatory reaction is not effectively suppressed during such diseases, such as acute lung injury (ALI) and COVID-19, an inflammatory storm occurs.[5−8] An inflammatory storm can result in sepsis with a considerably high mortality rate.[5] In the progression of ALI and COVID-19, inhibiting the development of inflammation is a highly effective treatment method. In the past three years of fighting against COVID-19, Chinese healthcare workers have adopted numerous natural resources or herbal prescriptions to alleviate the occurrence of inflammatory storms.[9,10] Furthermore, the related research has shown some herbs or natural products exhibited protective activity against ALI.[11−13] Therefore, searching for anti-inflammatory compounds with good properties from natural products is a considerably important process.

During our ongoing research on anti-inflammatory agents from natural resources, the roots of *C. fortunei* have attracted our attention. Previous phytochemical research on the aerial parts of *C. fortunei* has led to the isolation of various types of lindenane-dimers. Lindenane dimers are the most abundant bioactive compounds in *Chloranthus* plants[14−17] and can be classified as shizukaol-type, chlorahololide-type, and sarcano-

Received: May 8, 2024
Revised: July 24, 2024
Accepted: July 25, 2024
Published: August 2, 2024

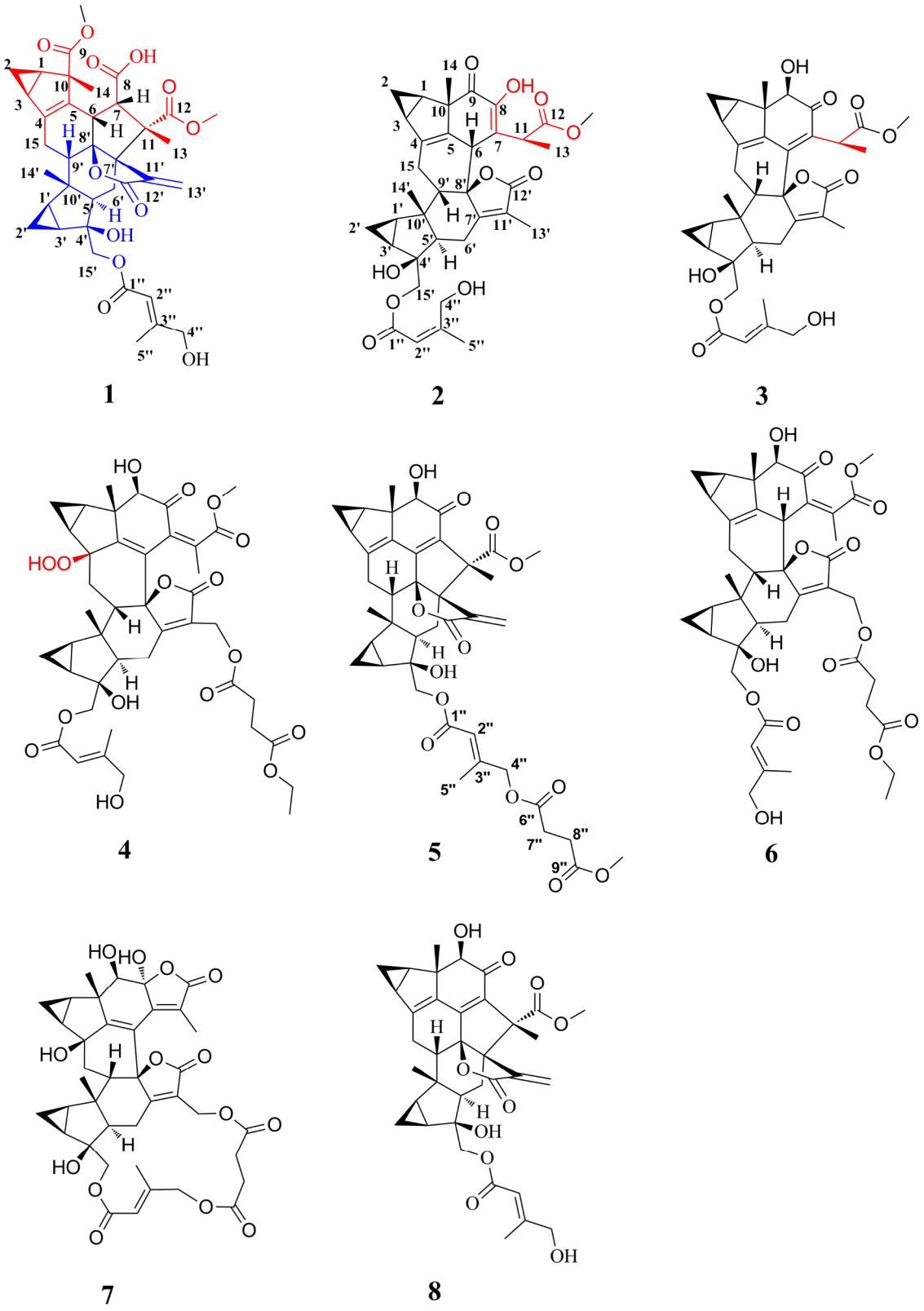

Figure 1. Compounds **1**−**8** isolated from roots of *Chloranthus fortunei*.

lide-type. Shizukaol-type dimers are the earliest type found and the most widely distributed; the two remaining types of dimers are relatively rare. In the past two decades, dozens of lindenane sesquiterpene dimers have been tested for their bioactivities; results have shown that these compounds display wide bioactivities, including antitumor, anti-inflammatory, antibacterial, neuroprotective, antiviral, and antimalarial activities. Based on our research on the roots of *C. holostegius* and *C. fortunei*,[18,19] we have developed a directional separation method of lindenane sesquiterpene dimers using HPLC-DAD methods. Using this method, we directionally isolated eight lindenane-type dimers, including five previously unre-

https://doi.org/10.1021/acsomega.4c04403
ACS Omega 2024, 9, 34869−34879

ported dimers (Figure 1). The results of anti-inflammatory activity evaluation showed that lindenane dimers have considerable potential for treating inflammatory diseases. Herein, we report the isolation and structure elucidation of lindenane sesquiterpenes as well as their biological activity evaluation.

2. EXPERIMENTAL SECTION

2.1. General Experimental Procedures. NMR spectra were recorded on a Bruker Avance III 500 NMR instrument (^{1}H, 500 MHz; ^{13}C, 125 MHz), with TMS as an internal standard. Mass spectra were recorded on a Dionex Ultimate 3000 UPLC-Q Exactive Plus (HR-ESI-MS). Silica gel (200−300 mesh, Qingdao Haiyang Chemical Co., Ltd., Qingdao, China) and RP-C18 (40−63 μm, Fuji, Japan) were used for column chromatography. Semipreparative HPLC was carried out using a Thermos N3000 series instrument with a Thermos Scientific Hypersil GOLD DIM RP-C18 column (10 × 250 mm, 4.6 μm) or a Shimadzu LC-20AR series instrument with a Shimpak RP-C_{18} column and an SPD-20A variable-wavelength detector.

2.2. Plant Material. The roots of *Chloranthus fortunei* were collected from Guangxi Province, China, and identified by Jin Xie from Anhui Medical University. A voucher specimen (no. 20180520) was deposited at the School of Pharmacy, Anhui Medical University.

2.3. Isolation and Purification. The powdered roots of *Chloranthus fortunei* (15.0 kg) were extracted at room temperature by using ethanol/H_2O (95/5, v/v) three times to afford a residue (696.0 g) after the solvent was removed. The residue was suspended in water and partitioned successively by petrol ether (PE) and ethyl acetate (EtOAc) to obtain PE-soluble (99.8 g) and EtOAc-soluble (476.9 g) fractions. The EtOAc-soluble fractions were subjected to silica gel column chromatography (CC, 600 mm × 100 mm) step gradient elution by CH_2Cl_2/CH_3OH (from 100:1, 50:1, 25:1, 15:1, 10:1, 5:1 to 0:1) to afford seven subfractions (Fr. EA-EG). Fr. EA (7.78 g) was subjected to silica gel CC (400 × 30 mm) eluted by PE/EtOAc (7:1−1:1) to obtain five subfractions (EA1-EA5). Fr. EA3−4 (1.2 g) was subjected to repeated silica gel CC (400 mm × 30 mm), ODS CC (400 mm × 50 mm, CH_3OH/H_2O, 50:50 v/v), Sephadex LH-20 gel CC (1500 mm × 15 mm, CH_3OH), and semipreparative HPLC (150 × 20 mm, 5 μm, flow rate 10 mL/min) to generate compound **1** (4.2 mg, t_R 17.4 min, CH_3OH/H_2O, 60:40 v/v) and compound **8** (6.2 mg, t_R 13.1 min, CH_3OH/H_2O, 60:40 v/v). Fr. EB (47.2 g) was subjected to silica gel CC (100 mm × 600 mm) eluted by CH_2Cl_2/CH_3OH to obtain 14 subfractions (EB1-EB14). Compounds **5** (12.0 mg, t_R 13.9 min, CH_3OH/H_2O, 60:40 v/v), **4** (5.1 mg, t_R 5.6 min, CH_3OH/H_2O, 60:40 v/v), **3** (10.4 mg, t_R 9.6 min, CH_3OH/H_2O, 60:40 v/v), and **2** (10.0 mg, t_R 16.8 min, CH_3OH/H_2O, 60:40 v/v) were obtained after repeated silica gel CC (400 mm × 30 mm, $CHCl_3$:CH_3OH), ODS CC (400 mm × 50 mm, CH_3OH/H_2O, 50:50 v/v), Sephadex LH-20 gel CC (1500 mm × 15 mm, CH_3OH), and semipreparative HPLC (20 × 150 mm, 5 μm, flow rate 10 mL/min). Fr. EC (50.5 g) was subjected to silica gel CC (600 mm × 100 mm) eluted by CH_2Cl_2/CH_3OH to obtain 14 subfractions (EC1-EC14). Compound **6** (3.7 mg, t_R 9.3 min, CH_3OH/H_2O, 50:50 v/v) and compound **7** (8.4 mg, t_R 11.4 min, CH_3OH/H_2O, 40:60 v/v) were obtained by repeated silica gel CC (400 mm × 30 mm, $CHCl_3$:CH_3OH), ODS CC (400 mm × 50 mm, CH_3OH/H_2O, 50:50 v/v), Sephadex LH-20 gel CC (1500 mm × 15 mm, CH_3OH), and semipreparative HPLC (20 × 150 mm, 5 μm, flow rate 10 mL/min).

2.4. Spectroscopic Data of Compounds. Fortunilide A (**1**): yellow amorphous powder. $[\alpha]^{20}_D$ −48.8 (*c* 0.9, CH_3OH). UV (CH_3OH): λ_{max} (log ε) 204 (4.67) nm. IR ν_{max} (KBr): 3505, 2925, 1735, 1725, 1663, 1630, 1604, 1155 cm^{-1}. ^{1}H and ^{13}C NMR data ($CDCl_3$), see Table 1. HRESIMS: *m*/*z* 703.2719 [M + Na]$^+$ (calcd for $C_{37}H_{44}O_{12}Na$, 703.2724).

Fortunilide B (**2**): yellow amorphous powder. $[\alpha]^{20}_D$ −39.9 (*c* 0.5, CH_3OH). UV (CH_3OH): λ_{max} (log ε) 202 (4.81), 283 (3.84) nm. IR ν_{max} (KBr): 3496, 2860, 1736, 1725, 1677, 1658, 1605, 1134 cm^{-1}. ^{1}H and ^{13}C NMR data ($CDCl_3$), see Table 1. HRESIMS: *m*/*z* 633.2581 [M−H]$^-$ (calcd for $C_{36}H_{41}O_{10}$, 633.2586).

Fortunilide C (**3**): yellow amorphous powder. $[\alpha]^{20}_D$ +10.2 (*c* 0.3, CH_3OH). UV (CH_3OH): λ_{max} (log ε) 204 (4.78), 283 (3.72), 350 (3.52) nm. IR ν_{max} (KBr): 3522, 2859, 1736, 1728, 1678, 1660, 1608, 1143 cm^{-1}. ^{1}H and ^{13}C NMR data ($CDCl_3$), see Table 1. HRESIMS: *m*/*z* 635.2849 [M + H]$^+$ (calcd for $C_{36}H_{43}O_{10}$, 635.2850).

Fortunilide D (**4**): White amorphous powder. $[\alpha]^{20}_D$ −22.4 (*c* 0.1, CH_3OH). UV (CH_3OH): λ_{max} (log ε) 202 (4.73), 280 (3.54) nm. IR ν_{max} (KBr): 3474, 2861, 1740, 1721, 1674, 1656, 1608, 1158 cm^{-1}. ^{1}H and ^{13}C NMR data ($CDCl_3$), see Table 2. HRESIMS: *m*/*z* 833.3025 [M + Na]$^+$ (calcd for $C_{42}H_{50}O_{16}Na$, 833.2991).

Fortunilide E (**5**): yellow amorphous powder. $[\alpha]^{20}_D$ −48.4 (*c* 1.9, CH_3OH). UV (CH_3OH): λ_{max} (log ε) 202 (4.90), 337 (3.83) nm. IR ν_{max} (KBr): 3550, 2967, 1742, 1727, 1684, 1662, 1636, 1147 cm^{-1}. ^{1}H and ^{13}C NMR data ($CDCl_3$), see Table 2. HRESIMS: *m*/*z* 747.3047 [M + H]$^+$ (calcd for $C_{41}H_{47}O_{13}$, 747.3011).

2.5. HPLC-HR-MS Analysis of the Crude Extracts. Liquid chromatography−mass spectrometry (LC−MS) was performed using a Dionex Ultimate 3000 and Thermo Q Exactive plus instrument. The ion source was electric spray ionization (ESI), and positive and negative ions were scanned alternately. The scanning mode was full scan data dependency two-stage scanning (full scan/ddMS2), with a scanning range of 100−1000 Da. The capillary temperature, spray voltage in negative mode, spray voltage in positive mode, sheath gas, and auxiliary gas were 350 °C, 3800 V, 3200 V, 35 arb, and 15 arb, respectively. MS2 used low, medium, and high collision energies with positive and negative ion modes set at 20, 40, and 60 V. The primary and secondary mass MS resolutions were FullScan 70000 fwhm (full width at half-maximum) and MS/MS 17500 fwhm, respectively. The obtained data were analyzed using Xcalibur (version 4.1).

2.6. Theoretical Calculations for ECD. The conformations of the compounds were examined by using the OPLS3 force field, followed by quantum chemical geometry optimization. Gaussian 16 was employed to geometrically optimize each conformation at the B3LYP/6-311G (2d, p) level. From these optimization results, the Boltzmann specific ratio for each conformation was determined. For the dominant conformation, 60 excited states were calculated using TD-DFT with the CAM-B3LYP/6-311G(2d,p) basis set. The ECD spectra were then analyzed using SpecDis software and compared to the experimental spectra.[20]

2.7. Theoretical Calculations for Fukui Function and Free Energy. The density functional theory (DFT) method was performed by using the Gaussian16 program. The B3LYP/

https://doi.org/10.1021/acsomega.4c04403
ACS Omega 2024, 9, 34869−34879

Table 1. ^{1}H and ^{13}C NMR Spectroscopic Data for Compounds 1−3[a]

	1		2		3	
no.	δ_H (mult)	δ_C	δ_H (mult)	δ_C	δ_H (mult)	δ_C
1	1.98 m	24.4	2.22 m	23.6	2.11 m	25.6
2	0.24 m	11.3	0.58 m	17.1	0.69 m	13.8
	0.88 m		1.08 m		1.09 m	
3	2.19 m	24.9	1.43 m	29.0	2.09 m	27.9
4		151.5		143.0		150.2
5		129.8		133.0		139.3
6	2.88 d (8.3)	48.8	3.80 s	45.3		142.1
7	3.14 m	58.6		119.1		130.3
8		171.8		146.5		199.5
9		180.7		199.8	4.36 s	79.1
10		57.7		57.7		53.5
11		59.0	2.75 q (7.5)	43.2	3.39 q (6.9)	38.8
12		174.5		172.7		173.6
13	1.23 s	30.2	1.47 d (7.5)	29.0	1.11 d (6.9)	18.3
14	1.37 s	20.6	1.28 s	24.8	0.99 s	17.4
15	2.63 m	25.1	2.71 m	26.1	2.84 m	27.0
	2.17 m		2.51 m			
1′	1.55 m	27.5	1.63 m	25.6	1.58 m	26.3
2′	0.58 m	15.0	0.64 m	11.5	0.75 m	12.3
	1.22 m		1.20 m		1.29 m	
3′	1.57 m	29.2	1.21 m	26.1	1.72 m	28.5
4′		79.6		77.3		77.7
5′	1.98 m	53.6	1.80 m	61.0	2.64 m	56.6
6′	3.00 m	33.5	2.55 m	26.5	2.49 m	21.9
	1.85 m		1.90 m		2.64 m	
7′		55.2		165.8		165.0
8′		99.6		92.5		85.7
9′	2.00 m	54.3	1.82 overlapped	59.6	1.94 dd (3.0, 7.5)	57.8
10′		41.6		44.7		44.3
11′		148.5		124.8		125.4
12′		169.0		173.4		172.5
13′	6.42 s	124.7	1.85 s	9.0	1.88 s	9.1
	6.06 s					
14′	0.77 s	21.7	0.80 s	25.5	0.95 s	26.5
15′	4.32 d (11.2)	70.4	4.05 d (12.0)	71.4	4.08 d (11.5)	67.9
	4.20 d (11.2)		3.76 d (12.0)		3.97 d (11.5)	
1″		166.7		166.8		166.6
2″	6.09 s	113.6	6.04 s	112.8	5.93 s	111.9
3″		157.8		159.4		160.4
4″	4.16 s	67.5	4.16 s	67.1	4.16 d (16.0)	66.9
					4.10 d (16.0)	
5″	2.09 s	15.7	2.12 s	15.9	2.05 s	15.8
9-OMe	3.83 s	53.4				
12-OMe	3.69 s	52.1	3.61 s	52.2	3.59 s	52.4

[a]Data (^{1}H 500 MHz, ^{13}C 125 MHz) in $CDCl_3$. δ: ppm, J in Hz.

Table 2. ^{1}H and ^{13}C NMR Spectroscopic Data for Compounds 4 and 5[a]

	4		5	
no.	δ_H (mult)	δ_C	δ_H (mult)	δ_C
1	2.12 m	26.1	2.17 dt (9.1, 4.9)	28.5
2	1.08 m	14.4	1.19 m	15.4
	0.67 m		0.63 m	
3	2.36 m	28.1	1.96 m	26.6
4		91.1		151.3
5		159.0		135.4
6		127.3		151.4
7		143.8		129.7
8		198.6		197.1
9	3.86 s	78.0	3.97 s	83.2
10		50.5		57.6
11		128.9		65.4
12		170.6		172.0
13	1.80 s	21.7	1.37 s	19.0
14	1.00 s	15.6	1.15 s	14.8
15	3.04 m	37.2	2.28 dd (17.9, 9.5)	29.2
			2.94 dd (18.0, 7.2)	
1′	1.57 m	27.6	1.63 m	26.6
2′	0.88 m	10.4	0.64 m	10.4
	1.20 m		1.19 m	
3′	1.78 m	23.1	1.64 m	29.7
4′		77.5		78.7
5′	2.69 m	56.1	1.57 dd (14.2, 2.8)	56.5
6′	2.60 m	24.5	2.52 dd (14.5, 7.2)	28.2
	2.57 m		1.72 d (14.3)	
7′		125.6		59.1
8′		87.8		95.5
9′	1.78 m	54.3	2.63 dd (9.5, 7.2)	52.1
10′		45.3		43.1
11′		166.5		146.1
12′		172.4		168.4
13′	5.09 d (13.5)	8.5	5.50 brs	122.9
	4.77 d (13.5)		6.18 brs	
14′	0.96 s	27.7	0.93 s	24.0
15′	4.04 d (12.0)	69.4	4.30 d (11.1)	70.4
	4.01 d (12.0)		4.07 d (11.1)	
1″		171.6		166.0
2″	5.90 m	111.7	5.90 m	114.4
3″		161.1		154.1
4″	4.18 d (15.0)	67.4	4.60 m	67.3
	4.14 d (15.0)			
5″	2.10 s	16.0	2.12 s	16.0
6″		170.1		171.7
7″	2.72 m	29.2	2.68 m	28.9
8″	2.61 m	28.8	2.73 m	29.0
9″		173.1		172.8
6″-OEt	4.11 q (7.5)	61.5		
	1.25 t (7.5)	29.7		
12-OMe	3.78 s	53.3	3.43 s	52.1
9″-OMe			3.69 s	52.1

[a]Data (^{1}H 500 MHz, ^{13}C 125 MHz) in $CDCl_3$. δ: ppm, J in Hz.

6-31G(d, p) theoretical model was adopted for all calculations. The potential energy surface scan was performed for reaction one, and the transition state was found, calculating the energy barrier. For reaction two, the QST1 method was used to find the transition state, and the reactants and products were verified through IRC calculations and also calculating the energy barrier.

2.8. Cell Culture. After inoculating the lung epithelial cell line MLE-12 cells at a density of 1×10^6 cells per well on a 6-well plate for 24 h. Then, the MLE-12 cells were stimulated

https://doi.org/10.1021/acsomega.4c04403
ACS Omega 2024, 9, 34869−34879

with LPS (50 mM) for 24 h before using for evaluation. Then, the cells were incubated in the presence or absence of various concentrations of isolates (1.0, 10.0, 100.0 μM), which was solubilized with DMSO for 24 h. Subsequently, the cell supernatant and MLE-12 cells were collected and stored at −20 °C for future use.

2.9. Cell Viability Tests. The cells were incubated in the presence or absence of various concentrations of isolates (1.0, 10.0, 100.0 μM), which was solubilized with DMSO for 24 h. Subsequently, the culture medium was removed. 200 μL of CCK-8 (0.5 mg/mL) was added to each well, and the mixture was incubated for 4 h. The supernatant was discarded and 150 μL of DMSO added to each well. The absorbance value of each well was measured at 490 nm using a microplate spectrophotometer. The experiment was paralleled three times, and dexamethasone was used as the positive control.

2.10. The ROS Tests. MLE-12 cells were stimulated with LPS (50 mM) for 24 h, and 7 (1, 10, 100 μM) was added and incubated for 24 h at concentrations of 1.0, 10.0, 100.0 μM. 2′,7′-Dichlorofluorescein diacetate (DCFH-DA) was used to detect intracellular ROS levels in MLE-12 cells. The instructions of the reagent kit were followed strictly.

2.11. Western Blotting Assays. Total protein was extracted from the lysate of MLE-12 cells, and the protein content was determined using the BCA method. SDS-PAGE electrophoresis was performed on protein samples and transferred onto PVDF membranes. 5% skim milk powder was sealed at room temperature for 2 h and incubated with the relevant primary antibodies (1:1000). The membrane was rinsed with TBST and reacted with the second antibody (1:500) coupled with horseradish peroxidase. The membrane was rinsed with TBST and then developed with an enhanced chemiluminescence (ECL) luminescent reagent. The optical density of the main band was measured using grayscale imaging software (UVP, UK) to calculate the expression of the aforementioned proteins in lung tissue.

2.12. Statistical Analysis. All data are expressed as the mean ± SD. The test was used to analyze the differences between sets of data with GraphPad Prism 8 software. All experiments were repeated at least three times.

3. RESULTS AND DISCUSSIONS

Fortunilide A (**1**) was isolated as an amorphous powder, with its molecular formula $C_{37}H_{44}O_{12}$ deduced from the HRESIMS ions observed at m/z 703.2719 $[M + Na]^+$ (calcd 703.2724), indicating 16 indices of hydrogen deficiency. The ^{1}H NMR spectrum (Table 1) indicated one singlet olefinic proton signal (δ_H 6.09), a pair of singlet terminal olefinic proton signals (δ_H 6.42 and 6.06), two oxygenated methyl groups (δ_H 3.83 and 3.69), and four tertiary methyl groups (δ_H 2.09, 1.37, 1.23, and 0.77). Two sets of characteristic cyclopropane upfield signals (δ_H 0.24, m and 0.58, m) indicated that compound **1** was a lindanane dimer.[18,19] The ^{13}C NMR spectra of compound **1** showed 37 carbon resonances, including five carbonyl carbon signals, six olefinic carbon signals, and four oxygenated carbon signals with the help of the DEPT Q spectra. The aforementioned data suggest that compound **1** is a lindenane dimer. Compound **1** was further elucidated by using HSQC and HMBC spectra (Figure 2). The characteristic singlet methyl group and the terminal olefinic protons revealed that **1** was a sarcanolide-type lindenane dimer, which was confirmed via HMBC correlations of H_3-13 to C-11, C-7′, and C-12; H-7 to C-6, C-8, C-13, C-11, and C-12; and H-13′ to C-7′, C-12′, and C-11′. The H-14′ to C-10′ and C-5′ and the H-15′ to C-3′ and C-4′ revealed the B unit (in blue in Figure 1) of compound **1**. Furthermore, the H-2″ to C-1″ and C-4″; H-4″ to C-5″; H-5″ to C-2″; and H-15′ to C-1″ revealed a 4-hydroxymethyl-1-butyryl located at C-15′. The HMBC correlations of H-13 to C-11, C-7′, and C-12; H-15 to C-3 and C-5; H-2 to C-4; H-3 to C-4; and H-6 to C-8′ and C-7 further demonstrated that compound **1** was a sarcanolide-type dimer. Finally, the HMBC correlation of H_3-14 to C-9, C-10, and C-5; H-1 to C-9; H-7 to C-8; and H_3−OCH_3 to C-9 built the planar structure of **1** as a novel 8/9-seco sarcanolide-type dimer. The relative structure of **1** was determined by the NOESY spectrum (Figure 2). The key correlation of H_3-13/H-7, H_3-13/H-6, and H_3-14/H-6 revealed the cofacial attribute of 13-CH_3, H-6, H-7, and 14-CH_3. The correlation of H_3-13 and H_2-13′ indicated that the lactone moiety was in the β-orientation. Furthermore, the correlation of H-6/H-9′, H-9′/H_3-14′, and H-2′/H_3-14′ and the correlation of H-1′/H-5′ and H-5′/H_2-15′ demonstrated the relative configuration of the B unit. Finally, the presence of a NOESY correlation of H-2″ and H-4″ revealed the *E* geometry of the 2″/3″ bond. The absolute configuration of compound **1** was determined via ECD calculations using time-dependent density functional theory (DFT). After a comparison of the calculated curve with the experimental curve (Figure 3A), we showed the absolute configuration of compound **1** to be 1*R*,3*S*,6*S*,7*R*,10*S*,11*S*,1′*R*,3′*S*,4′*S*,5′*R*,7′*R*,8′*R*,9′*S*,10′*S*. Compound **1** was the second example of a C-8/C-9 seco lindenane dimer, which was considered a product of the oxidation of 8/9-diketone. This type of lindenane dimer was first reported as sarglaroid A by the Luo group,[21] isolated from the roots of *Sarcandra glabra* (Thunb.) Nakai of the same family, Chloranthaceae.

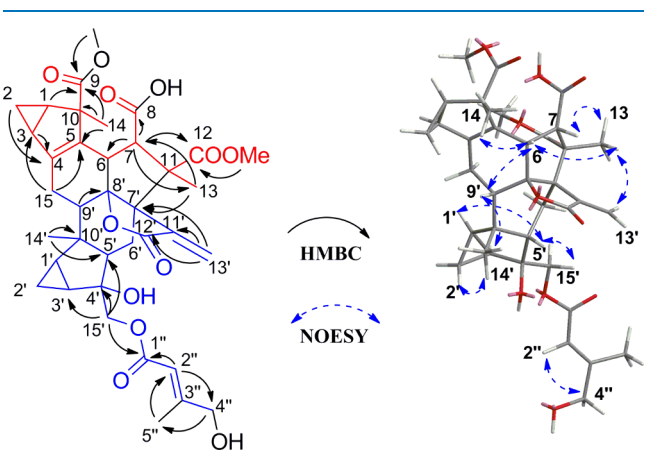

Figure 2. Key HMBC and NOESY correlation of compound **1**.

Compound **2** has the molecular formula $C_{36}H_{42}O_{10}$, deduced from the HR-ESI-MS ion peak observed at 633.2581 $[M-H]^-$ (calcd. 633.2586). The ^{1}H NMR spectrum (Table 1) revealed **2** was also a lindane dimer, indicated from the characteristic signals of 1,3-bisubstituted cyclopropane (δ_H 0.64, m and 0.58, m). The ^{1}H NMR and ^{13}C NMR spectra indicated that the structure of **2** closely resembled the known compound sarglaroid C.[21] The main difference between **2** and sarglaroid C was the substitution of small organic moieties at C-15′ (4-hydroxyl-5-methylbut-2-enoyl) and C-13′. These differences were further determined by HMBC correlation of H_3-13 to C-11, C-12, and C-7, H-4″ to C-2″, and C-3″, H-2″

https://doi.org/10.1021/acsomega.4c04403
ACS Omega 2024, 9, 34869−34879

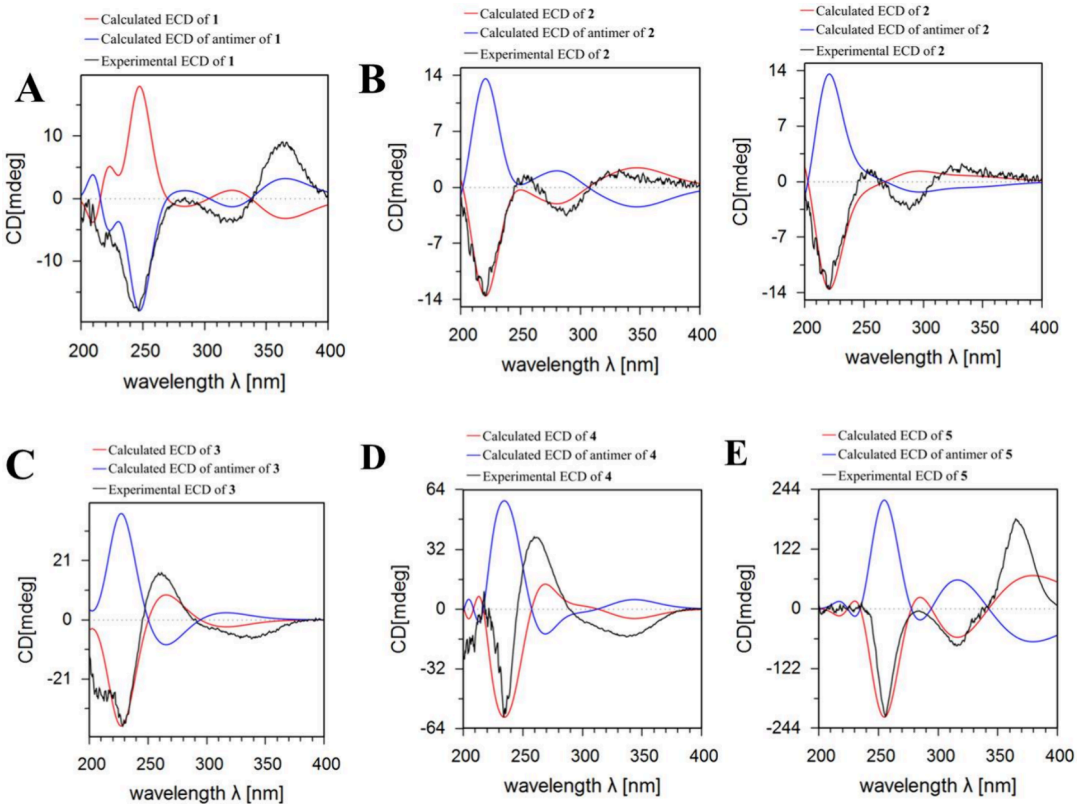

Figure 3. Calculated ECD and the experimental ECD of compounds **1**−**5**. (A) **1**; (B) left for 11*R*-conformation, right for 11*S*-conformation; (C) **3**; (D) **4**; (E) **5**.

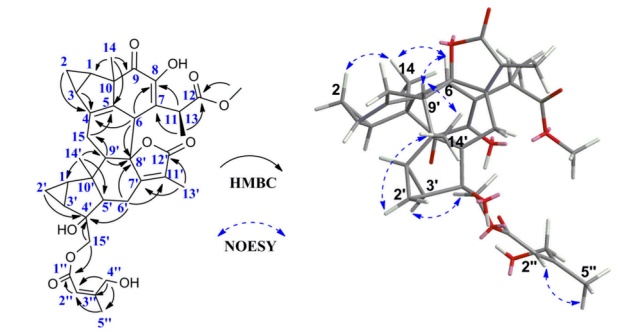

Figure 4. Key HMBC and NOESY correlation of compound **2**.

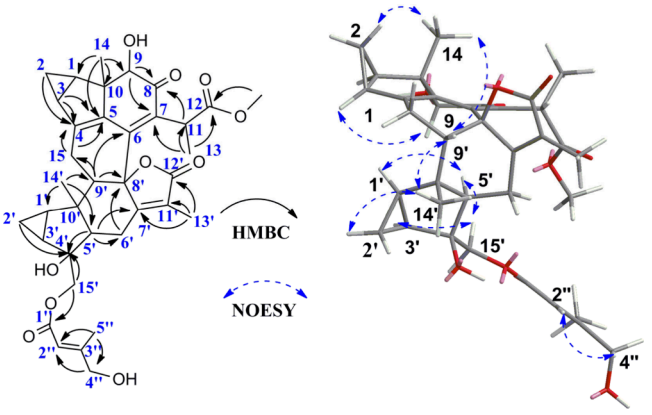

Figure 5. Key HMBC and NOESY correlation of compound **3**.

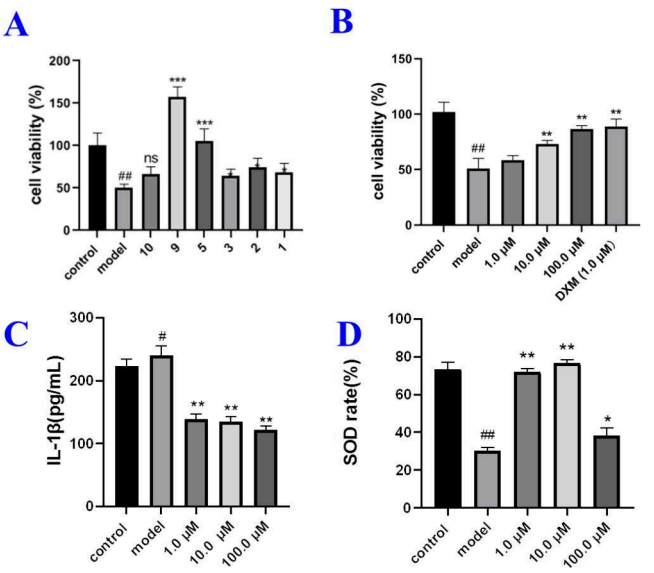

Figure 6. (A) The protective activity against LPS induced MLE-12 cells of compounds **1**−**3**, **5**, 7, and **8** (100.0 μM). (B) The protective activity of 7 in LPS stimulated MLE-12 cells of different concentrations at 1.0, 10.0, and 100.0 μM. Dexamethasone was used as a positive control. (C) Effects of 7 on the production of SOD in LPS stimulated MLE-12 cells. (D) Effects of 7 on the production of IL-1β in LPS stimulated MLE-12 cells ($^{\#}p < 0.05$ or $^{\#\#}p < 0.01$ versus the control group indicates statistically significant differences from the LPS group; $^{*}p < 0.05$ or $^{**}p < 0.01$ versus the LPS group).

to C-1″, and H-5″ to C-2″ (Figure 4). The relative configuration was determined by the NOESY spectrum (Figure 4), in which the correlation of H-2″ and H-5″

https://doi.org/10.1021/acsomega.4c04403
ACS Omega 2024, 9, 34869−34879

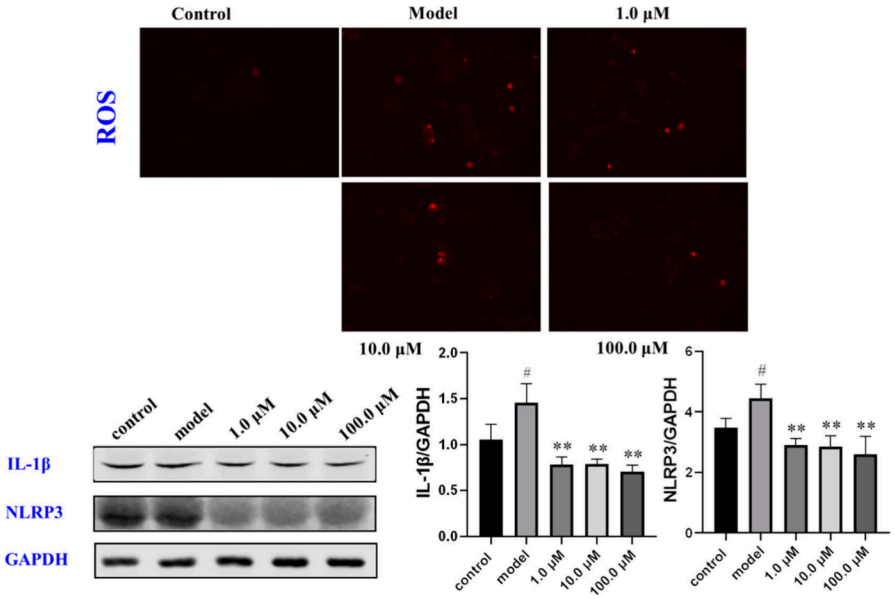

Figure 7. Result of the ROS measured using the chemiluminescence method (×100). Effects of **7** on the inhibition of IL-1β and NLRP3 in LPS-stimulated MLE-12 cells by Western blot (*p < 0.05 or **p < 0.01 versus LPS group, $^{\#}p$ < 0.05 versus the control group).

revealed the *Z* geometry of the C-2″/C-3″ double bond. As previously reported by the Luo group,[21] 13-CH_3 of this dimer of this type was β-oriented according to the NOESY correlation of H_3-14/H-6/H-11. The absolute configuration of compound **2** was elucidated by a comparison of DFT-calculated ECD and experimental ECD results (Figure 3B). Although the NOESY test can solve the relative configuration of 13-CH_3, it has certain drawbacks. Therefore, when calculating the ECD of the absolute configuration of the compound, we separately calculated the 11*S* and 11*R* configurations. Consequently, C-11 was determined as *R*, and the absolute configuration of the whole molecule. In studies aimed at solving the absolute configuration of such scaffolds, the ECD exciton chirality method is widely used. A right-handed helicity of two coupling chromophores, the π,π-conjugated system (C-7−C-8−C-9) and the γ-lactone (C-7′−C-11′−C-12′) could be derived from the ECD spectrum of **2**, demonstrating the absolute configuration of **2** as 8′*R*, which was consistent with the ECD calculation (Figure 3B).

Compound **3** has the same molecular formula $C_{36}H_{42}O_{10}$ as that of **2**, deduced from the HR-ESI-MS $[M + H]^+$ ion peak observed at 635.2849 (calcd. 635.2850). In the ^{1}H NMR spectrum (Table 1), the characteristic 1,3-bisubstituted cyclopropane signals (δ_H 0.69, m and 0.75, m) and a doublet methyl signal (δ_H 1.11, d, J = 6.90 Hz) indicated that **3** was a C-11 methine lindanane sesquiterpene dimer. The ^{1}H and ^{13}C NMR resonances indicated that the structure of **3** was considerably similar to that of the known compound chololactone G,[18] differing only in the small organic acid moiety at C-15′. The HMBC correlations (Figure 5) of H_3-13 to C-11, C-12, and C-7 and H_3-11 to C-12 and C-8 and C-6 confirmed the C-11 methine. Moreover, HMBC correlation of H-4″ to C-2″ and C-3″, H-2″ to C-1″, H-5″ to C-2″, and H_2-15′ to C-1″ revealed a 4-hydroxyl-5-methylbut-2-enoyl group located at C-15′. The NOESY correlation of H-2″/H-4″ determined the *E* geometry of the C-2″/C-3″ double bond. The absolute configuration of **3** was determined by using a DFT calculation. A comparison of the calculated and experimental ECD (Figure 3C), showed the absolute configuration of **3** to be 1*R*, 3*S*, 6*S*, 7*R*, 10*S*, 11*S*, 13*R*, 1′*R*, 3′*S*, 4′*S*, 5′*R*, 7′*R*, 8′*R*, 9′*S*, and 10′*S*. The absolute configuration of **3** was also confirmed by using the ECD exciton chirality method (Figure 3C).

Compound **4** was isolated as an amorphous powder, with its molecular formula $C_{42}H_{50}O_{16}$ deduced from the HRESIMS $[M + Na]^+$ ion peak observed at 833.3025 (calcd. 833.2991). The ^{1}H NMR and ^{13}C NMR spectra (Table 2) indicated that the structure of **4** closely resembled that of the known compound chlojaponilide F (**6**).[22] The only difference was the additional oxygenated carbon signal at δ_C = 91.1 and the two additional oxygen atoms in the molecular formula. The HMBC of H-3 to C-4 and H-15 to C-4 and C-5 revealed a hydroperoxyl at C-4; furthermore, the double bond at C-4/C-5 was shifted to C-5/C-6. Compound **4** was elucidated as a peroxidized lindanane-type dimer. The *E* geometry of $\Delta^{2''}$ was determined from the NOESY correlation of H-2″ and H-4″. At last, the absolute configuration of **4** was determined using the DFT calculation of the ECD spectrum (Figure 5D) as 1*R*, 3*S*, 6*S*, 7*R*, 10*S*, 11*S*, 1′*R*, 3′*S*, 4′*S*, 5′*R*, 7′*R*, 8′*R*, 9′*S*, 10′*S*. Both molecules of **4** and **6** have an ethoxy group, which is not commonly found in natural products. We analyzed the methanol extracts of the roots of *C. fortunei* using HPLC-MS and did not find any traces of them in the results (Supporting Information Part I). Therefore, compounds **4** and **6** can be considered as artificial products.

Compound **5** was obtained as a white, amorphous powder. Its molecular formula was determined to be $C_{41}H_{46}O_{13}$ from the HRESIMS $[M + H]^+$ ion peak at 747.3047 (calcd.747.3011). The ^{1}H and ^{13}C NMR spectra of **5** (Table 2) were considerably similar to those of the known compound fortunilide O.[23] The only difference was the additional methoxy group (δ_H = 3.69). The HMBC correlation of H_3−OCH_3 to C-9″ demonstrated that the additional methoxyl group was a signal of C-9″ methyoxl ester. The NOESY correlation of H-2″/H-4″ determined the *E* geometry of the C-2″/C-3″ double bond. The absolute configuration of **5** was also determined via DFT calculation of the ECD spectrum

https://doi.org/10.1021/acsomega.4c04403
ACS Omega 2024, 9, 34869−34879

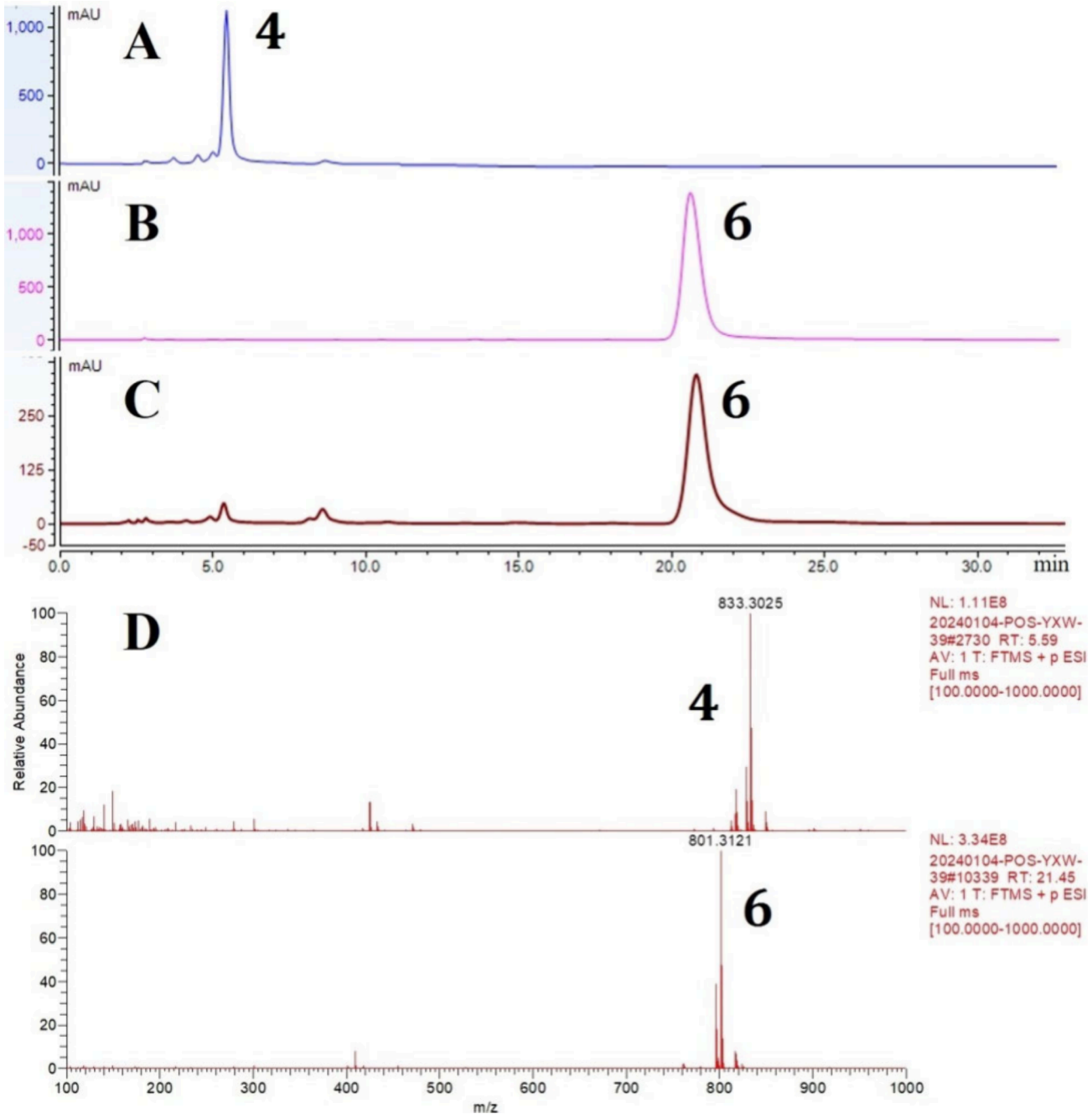

Figure 8. Confirmation of phenomena of the conversion between compounds **4** and **6**. (A) HPLC chromatography of **6** after 1 day of the purification. (B) HPLC chromatography of **6** after 1 week of the purification. (C) HPLC chromatography of **6** after one month of the purification. (D) The result of the UPLC-HR-MS analysis of **6** after one month of the purification.

(Figure 5E) as 1*R*, 3*S*, 6*S*, 7*R*, 10*S*, 11*S*, 1′*R*, 3′*S*, 4′*S*, 5′*R*, 7′*R*, 8′*R*, 9′*S*, 10′*S*.

Furthermore, the three compounds **6**−**8** were individually obtained and identified as chlojaponilide F (**6**),[22] chloramultilide B (**7**),[17] and fortulactone A (**8**),[18] respectively. For these methyl ester compounds (**1**−**3**, **5**, and **8**), we confirmed through LC-MS experiments that these compounds are not artificial products (Supporting Information Part I).

A previous study on the aerial parts of *Chloranthus fortunei* have led to the isolation of a series of anti-inflammatory lindenane sesquiterpene dimers with potential protective activity against ALI.[19] To the best of our knowledge, whole plants of *C. fortunei* were used as a traditional herb medicine for antibacterial and anti-inflammatory applications, promoting blood circulation, and dispersing blood stasis. To verify whether these compounds exert protective effects on ALI, the compounds with relatively large amounts (**1**−**3**, **5**, **7**, **8**) were evaluated for their protective activity against LPS-induced pulmonary epithelial cell line-12 (MLE-12). Results indicated that **7** showed the most potential protective activity (Figure 6). After LPS stimulation, MLE-12 cells were affected by reactive oxygen species (ROS), resulting in cell damage.[24,25] The results of immunofluorescence experiments demonstrated that **7** can effectively reduce the impact of ROS, thereby reducing the level of inflammatory damage (Figure 7). Moreover, we further validated the activity of compound **7**. An ELISA

https://doi.org/10.1021/acsomega.4c04403
ACS Omega 2024, 9, 34869−34879

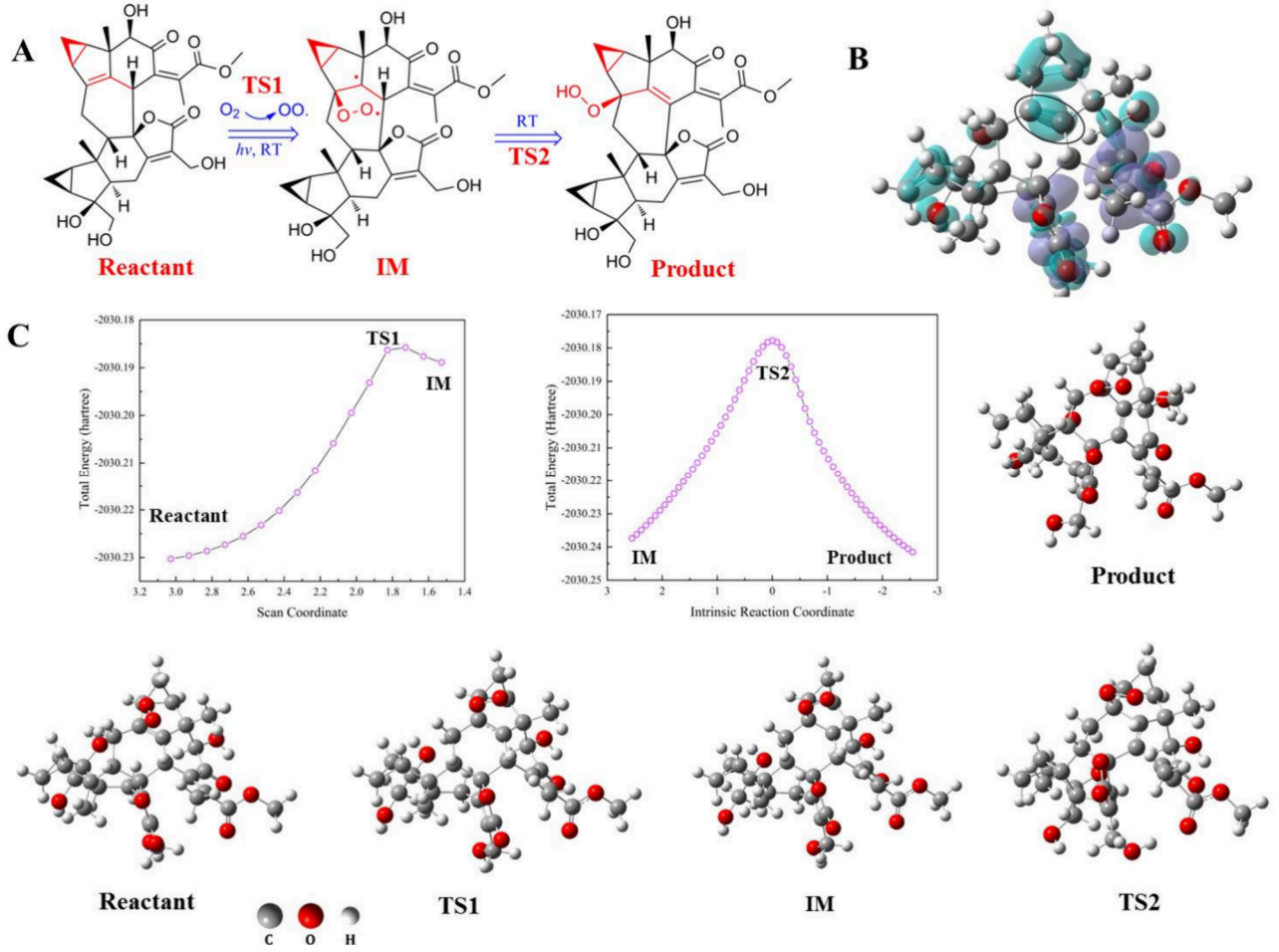

Figure 9. (A) The proposed "decayed" pathway of the Shizukaols model dimer. (B) The calculation result is the Fukui function of reactant. (C) The free energy of the pathway was calculated by DFT. TS and IM are the abbreviations for transition state and intermediate, respectively.

experiment involving **7** showed that it can effectively inhibit the generation of the inflammatory factor IL-1β in cells and promote the generation of SOD (Figure 6).[26,27] IL-1β is a key cytokine in the pulmonary inflammatory response process,[28,29] which is confirmed via Western blotting experiments. The expression of IL-1β is regulated by the inflammasome NLRP3 (Figure 7).[30−32] The expression of NLRP3 was significantly inhibited, as deduced from the Western blotting results. Although we endeavored to attempt to identify pathways associated with NLRP3 to further investigate the biological activity of **7**, all attempts were unsuccessful.

Based on the structural aspects of these compounds, as depicted, the isolates cover almost all types of such compounds. Lindenane-type dimers are structurally complex natural products with diversified bioactivities. These types of dimers have been partly artifact synthesized, such as shizukaol-type dimers.[33] As our previously reported,[34] the peroxidized chlorahololide-type dimer was considered an artifact generated from the peroxidation of the shizukaol-type dimers. To confirm this, HPLC-HR-MS was employed to analyze the crude extract of the roots of *C. fortunei*. No traces of **4** were found in the crude extracts of the roots of this plant. To further confirm this conjecture, a shizukaol-type dimer, **6**, was deposited in $CDCl_3$ for 1 day, 1 week, and one month. Subsequently, we conducted HPLC or HPLC-MS detection at the three time points. Compound **4** appeared at the very beginning of the retention time in the HPLC chromatograph from the first day onward (Figure 8), indicating that **4** was an artifact generated from the results of free radical reactions of **6** (Figure 9A). As previously reported, the small organic acid esters at C-15′ and C-13′ of unit B had no decisive effect on the changes in compounds. Although we explained this mechanism in the paper, we acknowledge with regret that we have not comprehensively explained the reactivity of the double bond of C-4/C-5 of shizukaol-type sesquiterpene dimers and the transition states of the reaction. In our previous paper, we elucidated that small molecule acids do not play a crucial role in the progress of the reaction.[34] Thus, we simplified the substituents at C-15′ and C-13′ for ease of calculation. Based on the DFT calculation, the Fukui function was expressed as a contour map of the orbital weight double descriptor (Figure 9B). The purple part is prone to electrophilic reactions, whereas the blue part is prone to nucleophilic reactions, revealing that the C4/C5 double bond of shizukaol-type lindenane dimers is easy to oxidize. We used DFT calculations to determine the transition state of this reaction (Figure 9C). First, the substrate produces C-4 peroxide free radical intermediates with oxygen free radicals. In this step, two intermediates should be generated (4-α type or β type). We obtained a stable structure 4β type intermediate through structural optimization calculations using Gaussian at the B3LYP/6-31G (d, p) level and verified the absence of a 4α type intermediate in imaginary frequencies through frequency calculation. Thus, 4α type intermediates cannot be produced. In the latter half of this reaction, a

https://doi.org/10.1021/acsomega.4c04403
ACS Omega 2024, 9, 34869−34879

transition state forms between the peroxide group and the hydrogen atom at the C-6 position. Subsequently, C-6 hydrogen atoms are transferred to the peroxide group, producing the final peroxide product. This transition state indicates that in order to form a C-4 peroxide hydroxyl product, the aforementioned peroxide group must be cofacial with the C-6 hydrogen atom. Therefore, only the final peroxide product 4β-OOH is reported in the literature.

4. CONCLUSIONS

Collectively, eight lindanane sesquiterpene dimers were isolated from the roots of *C. fortunei*, and their structural significances were summarized. Among these, compound **7** was proven to be the most potent protective molecule against LPS-induced pulmonary epithelial cell lines. Further biological evaluation *in vitro* demonstrated that **7** reduced the production of ROS and IL-1β which are regulated by the expression of NLRP3. These results demonstrated the therapeutic potential of compound **7** in lung inflammatory diseases.

■ ASSOCIATED CONTENT

Supporting Information

The Supporting Information is available free of charge at https://pubs.acs.org/doi/10.1021/acsomega.4c04403.

Complementary experiments confirming that if compounds **1**−**6** and **8** are artifacts generated during the purification and storage process, HR-ESI-MS spectra, 1D and 2D NMR spectra, the Fukui function and free energy calculation details of the shizukaol model, and ECD calculation details for compounds **1**−**5** (PDF)

■ AUTHOR INFORMATION

Corresponding Authors

Bing-Yuan Yang − *Guangxi Key Laboratory of Plant Functional Phytochemicals and Sustainable Utilization, Guangxi Institute of Botany, Guangxi Zhuang Autonomous Region and Chinese Academy of Sciences, Guilin 541006, People's Republic of China*; Email: yby@gxib.cn

Chuan-Pu Shen − *Anhui Provincial Laboratory of Inflammatory and Immunity Disease, Anhui Institute of Innovative Drugs, School of Pharmacy, Anhui Medical University, Hefei 230032, People's Republic of China*; orcid.org/0000-0001-6896-4541; Email: 2016500001@ahmu.edu.cn

Authors

Xiu-Wen Yin − *Anhui Provincial Laboratory of Inflammatory and Immunity Disease, Anhui Institute of Innovative Drugs, School of Pharmacy, Anhui Medical University, Hefei 230032, People's Republic of China*

Jun-Jie Hu − *Anhui Provincial Laboratory of Inflammatory and Immunity Disease, Anhui Institute of Innovative Drugs, School of Pharmacy, Anhui Medical University, Hefei 230032, People's Republic of China*

Fu-Cai Ren − *Anhui Provincial Laboratory of Inflammatory and Immunity Disease, Anhui Institute of Innovative Drugs, School of Pharmacy, Anhui Medical University, Hefei 230032, People's Republic of China*

Xiang-Dong Pu − *Anhui Provincial Laboratory of Inflammatory and Immunity Disease, Anhui Institute of Innovative Drugs, School of Pharmacy, Anhui Medical University, Hefei 230032, People's Republic of China*; orcid.org/0000-0002-0892-035X

Meng-Yu Yang − *Anhui Provincial Laboratory of Inflammatory and Immunity Disease, Anhui Institute of Innovative Drugs, School of Pharmacy, Anhui Medical University, Hefei 230032, People's Republic of China*

Peng Wang − *School of Pharmacy, Yancheng Teachers University, Yancheng 224007, China*

Complete contact information is available at: https://pubs.acs.org/10.1021/acsomega.4c04403

Author Contributions

‖Contributed equally to this work. The manuscript was written through contributions of all authors. All authors have given approval to the final version of the manuscript.

Notes

The authors declare no competing financial interest.

■ ACKNOWLEDGMENTS

This research work was supported by the National Natural Science Foundation of China (31900285), Natural Science Project of Anhui Provincial Education Department (KJ2021A0235), Open Project of Jiangsu Key Laboratory for Bioresources of Saline Soils (JKLBS2017013), and The Youth Science Fund Project of Anhui Medical University (2023xkj011). The authors also thank Dr. Sheng Wang of the Center for Scientific Research of Anhui Medical University for valuable help in our experiment.

■ REFERENCES

(1) Editorial Committee of the Administration Bureau of Traditional Chinese Medicine. In *Chinese Materia Medica (Zhonghua Benchao)*; Shanghai Science & Technology: Shanghai, 1998; vol 3, pp 449−450.

(2) Yuan, T.; Zhu, R. X.; Yang, S. P.; Zhang, H.; Zhang, C. R.; Yue, J. M. Serratustones A and B Representing a New Dimerization Pattern of Two Types of Sesquiterpenoids from *Chloranthus serratus*. *Org. Lett.* **2012**, *14*, 3198−3201.

(3) Zhou, B.; Liu, Q. F.; Dalal, S.; Cassera, M. B.; Yue, J. M. Fortunoids A-C, Three Sesquiterpenoid Dimers with Different Carbon Skeletons from *Chloranthus fortunei*. *Org. Lett.* **2017**, *19*, 734−737.

(4) Chi, J.; Xu, W. J.; Wei, S. S.; Wang, X. B.; Li, J. X.; Gao, H. L.; Kong, L. Y.; Luo, J. Chlotrichenes A and B, Two Lindenane Sesquiterpene Dimers with Highly Fused Carbon Skeletons from *Chloranthus holostegius*. *Org. Lett.* **2019**, *21*, 789−792.

(5) Huang, C.; Wang, Y.; Li, X.; Ren, L.; Zhao, J.; Hu, Y.; et al. Clinical features of patients infected with 2019 novel coronavirus in Wuhan, China. *Lancet* **2020**, *395*, 497−506.

(6) Karki, R.; Kanneganti, T. D. The 'cytokine storm': molecular mechanisms and therapeutic prospects. *Trends Immunol* **2021**, *42*, 681−705.

(7) Zheng, Z.; Peng, F.; Xu, B.; Zhao, J.; Liu, H.; Peng, J.; Li, Q.; Jiang, C.; Zhou, Y.; Liu, S.; Ye, C.; Zhang, P.; Xing, Y.; Guo, H.; Tang, W. Risk factors of critical & mortal COVID-19 cases: a systematic literature review and meta-analysis. *J. Infect.* **2020**, *81*, e16−25.

(8) Karki, R.; Kanneganti, T. D. Innate immunity, cytokine storm, and inflammatory cell death in COVID-19. *J. Transl. Med.* **2022**, *20*, 542.

(9) Qi, F. H.; Tang, W. Traditional Chinese medicine for treatment of novel infectious diseases: Current status and dilemma. *Biosci. Trends* **2021**, *15*, 201−204.

(10) Xia, K. Y.; Zhao, Z. Y.; Shah, T. F.; Wang, J. Y.; Baloch, Z. Composition, Clinical Efficiency, and Mechanism of NHC-Approved "Three Chinese Medicines and Three Chinese Recipes" for COVID-19 Treatment. *Front. Pharmacol.* **2022**, *12*, No. 781090.

(11) Yao, L.; Hou, G.; Wang, L.; Zuo, X. S.; Liu, Z. Protective effects of thymol on LPS-induced acute lung injury in mice. *Microb. Pathog.* **2018**, *116*, 8−12.
(12) Bai, Z. F.; Li, P. Y.; Wen, J. C.; Han, Y. Z.; Cui, Y. Y.; Zhou, Y. F.; Shi, Z.; Chen, S. S.; Li, Q.; Zhao, X.; Wang, Z. X.; Li, R. S.; Guo, Y. M.; Zhan, X. Y.; Xu, G.; Ding, K. X.; Wang, J. B.; Xiao, X. H. Inhibitory effects and mechanisms of the anti-covid-19 traditional Chinese prescription, Keguan-1, on acute lung injury. *J. Ethnopharmacol.* **2022**, *285*, No. 114838.
(13) Zhong, R. X.; Xia, T. Y.; Wang, Y.; Ding, Z. H.; Li, W.; Chen, Y.; Peng, M. M.; Li, C. Q.; Zhang, H.; Shu, Z. P. Physalin B ameliorates inflammatory responses in lipopolysaccharide-induced acute lung injury mice by inhibiting NF-κB and NLRP3 via the activation of the PI3K/Akt pathway. *J. Ethnopharmacol.* **2022**, *284*, No. 114777.
(14) Zhan, Z. J.; Ying, Y. M.; Ma, L. F.; Shan, W. G. Natural disesquiterpenoids. *Nat. Prod. Rep.* **2011**, *28*, 594−629.
(15) Xu, Y. J. Phytochemical and Biological Studies of *Chloranthus* Medicinal Plants. *Chem. Biodivers.* **2013**, *10*, 1754−1773.
(16) Kawabata, J.; Fukushi, E.; Mizutani, J. Sesquiterpene Dimers from *Chloranthus japonicus*. *Phytochemistry* **1995**, *39*, 121−125.
(17) Xu, Y. J.; Tang, C. P.; Ke, C. Q.; Zhang, J. B.; Weiss, H. C.; Gesing, E. R.; Ye, Y. Mono- and Di-sesquiterpenoids from *Chloranthus spicatus*. *J. Nat. Prod.* **2007**, *70*, 1987−1990.
(18) Shen, C. P.; Luo, J. G.; Yang, M. H.; Kong, L. Y. Sesquiterpene dimers from the roots of *Chloranthus holostegius*. *Phytochemistry* **2017**, *137*, 117−122.
(19) Bian, X. X.; Zhao, X.; Liu, S. S.; Wu, L.; Yin, X. W.; Shen, C. P. Sesquiterpene dimers from *Chloranthus fortunei* and their protection activity against acute lung injury. *Fitoterapia* **2022**, *159*, No. 105191.
(20) Bruhn, T.; Schaumlöffel, A.; Hemberger, Y.; Bringmann, G. SpecDis: Quantifying the Comparison of Calculated and Experimental Electronic Circular Dichroism Spectra. *Chirality* **2013**, *25*, 243−249.
(21) Sun, Y. P.; Li, Y. Q.; Cui, L. T.; Li, Q. R.; Wang, S. Y.; Chen, Z. H.; Kong, L. Y.; Luo, J. Anti-Inflammatory Lindenane Sesquiterpenoid Dimers from the Roots of *Sarcandra glabra*. *J. Agri. Food Chem.* **2023**, *71*, 14000−14012.
(22) Guo, P. J.; Chen, T.; Hu, X. G.; Duan, Y. L.; Zheng, L.; Du, G. X.; Wang, Q.; Ding, A. X.; Qin, G. Q.; Chen, Y. H.; Wang, W. Q.; Mu, Q.; Xuan, L. J. Lindenane sesquiterpenoid dimers from *Chloranthus japonicus* improve LDL uptake by regulating PCSK9 and LDLR. *Bioorg. Chem.* **2024**, *142*, No. 106958.
(23) Wang, S. Y.; Li, Y. Q.; Wang, X. L.; Zhang, X. Q.; Xu, F.; Ying, P.; Kong, L. Y.; Luo, J. Fortunilides M-O, anti-inflammatory lindenane sesquiterpenoid dimers from *Chloranthus fortunei*. *Fitoterapia* **2023**, *168*, No. 105547.
(24) Ren, Y.; Yang, Z.; Sun, Z.; Zhang, W.; Chen, X.; Nie, S. Curcumin relieves paraquat-induced lung injury through inhibiting the thioredox in interacting protein/NLR pyrin domain containing 3-mediated inflammatory pathway. *Mol. Med. Rep.* **2019**, *20*, 5032−5040.
(25) Meng, M. Digitoflavone (DG) attenuates LPS-induced acute lung injury through reducing oxidative stress and inflammatory response dependent on the suppression of TXNIP/NLRP3 and NF-κB. *Biomed Pharmacother* **2017**, *94*, 712−725.
(26) Pang, X. R.; Shao, L. L.; Nie, X. J.; Yan, H. Y.; Li, C.; Yeo, A. J.; Lavin, M. F.; Xia, Q.; Shao, H.; Yu, G. C.; Jia, Q.; Peng, C. Emodin attenuates silica-induced lung injury by inhibition of inflammation, apoptosis and epithelial-mesenchymal transition. *Int. Immunopharmacol* **2021**, *91*, No. 107277.
(27) Impellizzeri, D.; Esposito, E.; Mazzon, E.; Paterniti, I.; Di Paola, R.; Bramanti, P.; Cuzzocrea, S. Effect of apocynin, a NADPH oxidase inhibitor, on acute lung inflammation. *Biochem. Pharmacol.* **2011**, *81*, 636−648.
(28) Wang, J.; Liu, Y. T.; Xiao, L.; Zhu, L. P.; Wang, Q. J.; Yan, T. H. Anti-Inflammatory Effects of Apigenin in Lipopolysaccharide-Induced Inflammatory in Acute Lung Injury by Suppressing COX-2 and NF-kB Pathway. *Inflammation* **2014**, *37*, 2085−2090.
(29) Lou, T.; Jiang, W. J.; Xu, D. H.; Chen, T.; Fu, Y. L. Inhibitory Effects of Polydatin on Lipopolysaccharide-Stimulated RAW 264.7 Cells. *Inflammation* **2015**, *38*, 1213−1220.
(30) Qu, J. R.; Wang, W.; Zhang, Q. J.; Li, S. Inhibition of Lipopolysaccharide-Induced Inflammation of Chicken Liver Tissue by Selenomethionine via TLR4-NF-κB-NLRP3 Signaling Pathway. *Biol. Trace Elem. Res.* **2020**, *195*, 205−214.
(31) Kim, S. K.; Choe, J. Y.; Park, K. Y. TXNIP-mediated nuclear factor-κB signaling pathway and intracellular shifting of TXNIP in uric acid-induced NLRP3 inflammasome. *Biochem. Biophys. Res. Commum.* **2019**, *511*, 725−731.
(32) Fouad, A. A.; Abdel-Aziz, A. M.; Hamouda, A. A. H. Diacerein Downregulates NLRP3/Caspase-1/IL-1β and IL-6/STAT3 Pathways of Inflammation and Apoptosis in a Rat Model of Cadmium Testicular Toxicity. *Biol. Trace Elem. Res.* **2020**, *195*, 499−505.
(33) Wu, J. L.; Lu, Y. S.; Tang, B. C.; Peng, X. S. Total syntheses of shizukaols A and E. *Nat. Commun.* **2018**, *9*, 4040.
(34) Yin, X. W.; Zhang, M.; Wu, L.; Ren, F. C.; Yang, F. R.; Pu, X. D.; Zhang, Z. J.; Shen, C. P. Anti-Inflammatory Peroxidized Chlorahololide-Type Dime-rs Are Artifacts of Shizukaol-Type Dimers: From Phenomena Discovery and C-onfirmation to Potential Underlying Mechanism. *Molecules* **2024**, *29*, 909.

https://doi.org/10.1021/acsomega.4c04403
ACS Omega 2024, 9, 34869−34879